

Final-State Interactions in $(e, e'p)$ Reactions with Polarized Nuclei

J.E. Amaro¹ and T.W. Donnelly²

¹ *Departamento de Física Moderna, Universidad de Granada, Granada 18071, Spain*

² *Center for Theoretical Physics, Laboratory for Nuclear Science and Dept. of Physics,
Massachusetts Institute of Technology, Cambridge, MA 02139, U.S.A.*

Abstract

The cross section for coincidence, quasielastic proton knock-out by electrons from a polarized ^{39}K nucleus is computed in DWIA using an optical potential in describing the wave function of the ejected nucleon. The dependence of the FSI on the initial polarization angles of the nucleus is analyzed and explained in a new, semi-classical picture of the reaction in which the nuclear transparency decreases as a function of the amount of nuclear matter that the proton has to cross, thus providing a method for obtaining detailed information on its mean free path in finite nuclei. We propose a procedure to find the best initial kinematical conditions for minimizing the FSI which will be useful as a guide for future experiments with polarized nuclei.

PACS: 25.30.Fj, 24.70.+s, 24.10.Ht, 21.60.Cs

Keywords: Nuclear reactions; Exclusive quasielastic electron scattering; Polarized nuclei; Optical potential; Mean free path; Nuclear transparency; Single-particle distributions.

MIT/CTP#2784

October 1998

1 Introduction

The interpretation of many experiments in nuclear physics requires an understanding of how nucleons propagate through nuclei [1, 2]. In particular, in quasi-free coincidence ($e, e'p$) reactions, an electron transfers an energy ω to a nucleon in the nucleus. This high-energy nucleon exits from the nucleus, leaving the daughter nucleus in a state with definite energy and momentum. The main effect of the final-state interaction (FSI) felt by the ejected nucleon as it travels across the residual nucleus is a reduction of the cross section due to attenuation caused by interactions with the nuclear matter through which the nucleon must propagate [3]. This attenuation can be described in terms of a complex one-body optical potential, whose imaginary part accounts for the loss of flux produced by transitions to channels other than the elastic one. Accordingly, it is expected that the so-called distorted wave impulse approximation (DWIA) yields a cross section which is smaller than in the plane-wave impulse approximation (PWIA), and hence that the nuclear transparency, defined as the ratio between the DWIA and PWIA cross sections, is usually less than one. This reduction is observed in experiments for low [3], moderate [1, 2] and high momentum transfer [4, 5], and at present there is no unambiguous evidence of a restoration of the full nuclear transparency (i.e., a reduction of the FSI) by effects such as those that underlie the idea of color transparency [6].

In this paper we explore the effects of the FSI in ($e, e'p$) reactions using polarized nuclei. The importance of having the FSI under control is clear if one is trying to study nuclear properties (such as initial-state momentum distributions) or reaction mechanisms (such as specifics of the nuclear electromagnetic current). All of the measurements mentioned above involving medium and heavy nuclei have been performed with unpolarized targets and hence only the global effects of FSI averaged over all polarization directions have been addressed experimentally to date. Using instead polarized nuclei as targets, new possibilities to extract the full tri-dimensional momentum distribution of nuclei will become available [7, 8, 9, 10]; of course, as in the unpolarized case, the FSI also enter here and must be taken into account.

In fact, as established in a previous paper [11], the various multipole reduced responses that enter as components of the cross section show different sensitivities to the FSI. Hence it is expected that there should be a dependence of FSI effects — or nuclear transparency — on the choice of polarization angles. There are only a few preliminary studies of ($e, e'p$) reactions involving polarized, medium and heavy nuclei in DWIA [9, 12], and these report only a few examples for illustrative purposes without developing detailed insights into the roles played by FSI for different polarizations.

Hence a theoretical study of such effects is motivated when attempting to understand the new issues of nuclear transparency as a function of the orientation of the nuclear spin. The goal of the present work is to show how the variations of the transparency can be understood in terms of the orientation of the initial-state nucleon's orbit (the one that in our model primarily carries the nuclear polarization) and of the attenuation of the

ejected nucleon's flux through its dependence on the length of the path that it travels in the nucleus. Although the method we follow is developed here for the particular case of the ejection of a proton from the $d_{3/2}$ shell of polarized ^{39}K leaving $^{38}\text{Ar}_{g.s.}$ as the daughter nucleus, it can be generalized for use with any polarized nucleus and can be addressed using more sophisticated nuclear models. The present choice is, however, prototypical. Using it we shall show that one is able to predict the orientations of the target polarization that are optimal for minimizing the FSI effects, that is, to make the nucleus as “transparent” as possible. As in these cases the FSI effects are minimized, they provide the ideal situations to study other issues such as specifics of initial-state nuclear structure. As we shall show below, this special situation occurs when the nucleon is ejected directly away from the nuclear surface. On the other hand, when the nucleon is ejected from the nuclear surface but in the opposite direction — into the nucleus — it has to cross the entire nucleus to exit on the opposite side, and the FSI effects are then found to be maximal (that is, one has the minimum transparency). This second situation is ideal for detailed studies of the imaginary, absorptive part of the FSI. Finally, intermediate situations arise in which the nucleon is ejected from the surface in a direction roughly “tangent” to the nuclear surface, and there the re-scattering mechanisms that originate with the real and spin-orbit parts of the potential have a major influence. All of these situations can be selected simply by changing the direction of the nuclear polarization. If one focuses on the first and second situations, but not the third in which re-scattering is appreciable, it is possible to parametrize the transparency in terms of a mean free path for *finite* nuclei.

The organization of the present work is as follows: in sect. 2 we review the details of the formalism for describing $(e, e'p)$ reactions with polarized nuclei which are of relevance for the discussions to follow, and present our model with some of the details of the calculation. In sect. 3 we show the numerical results of the present calculation of the cross section for different nuclear polarizations. In sect. 4 we introduce a semi-classical model of the reaction in order to provide a physical picture of the dependence presented in sect. 3 of the nuclear transparency as a function of the polarization angles and to parametrize it in terms of an effective mean free path. Finally, in sect. 5 we draw our conclusions.

2 Coincidence cross section of polarized nuclei

2.1 Kinematics and cross section

First we introduce the definitions of the kinematics we use. An electron is scattered by a nucleus $|A\rangle$ of mass M_A , transferring to it an energy $\omega = E_e - E'_e$ and momentum $\mathbf{q} = \mathbf{k}_e - \mathbf{k}'_e$. In the final state a proton of mass M with momentum \mathbf{p}' and energy E' is detected in coincidence with the electron. The daughter nucleus is left in a definite state

$|B\rangle$ with mass M_B^* , which we consider to be located in the discrete spectrum; accordingly we integrate over the missing energy

$$\begin{aligned} E_m &= \sqrt{(\omega + M_A - E')^2 - (\mathbf{q} - \mathbf{p}')^2} - M_B \\ &= \sqrt{E_B^2 - p_B^2} - M_B \equiv M_B^* - M_B, \end{aligned} \quad (1)$$

in order to select one of the discrete final states for B in the missing-energy spectrum. Here M_B is the daughter ground-state mass. Thus $E_B = \omega + M_A - E'$ is the total energy of the residual nucleus, $\mathbf{p} = -\mathbf{p}_B = \mathbf{p}' - \mathbf{q}$ is the missing momentum, and $M_B^* = \sqrt{E_B^2 - p_B^2}$ is the mass of the daughter nucleus in its (in general) excited state; we neglect recoil in the present work.

In addition, we consider the initial nucleus to be 100% polarized in a direction given by the unit vector $\boldsymbol{\Omega}^*$; that is, the initial hadronic state is labeled

$$|A\rangle = |A(\boldsymbol{\Omega}^*)\rangle = R(\boldsymbol{\Omega}^*)|J_i J_i\rangle, \quad (2)$$

where $R(\boldsymbol{\Omega}^*)$ is a rotation operator which maps the z -axis (the \mathbf{q} -direction) onto the $\boldsymbol{\Omega}^*$ direction and J_i is the total spin of the nucleus A . For simplicity in the following arguments, in this work we do not consider polarized electrons, since only the polarization of the nucleus is essential for the model presented in sect. 4; also in the present work the polarization of the final state is assumed not to be specified.

Assuming plane waves for the electrons and working in a reference system where the z -axis points in the positive \mathbf{q} direction and the x -axis is in the electron scattering plane, one has the following expression for the cross section [13]:

$$\Sigma \equiv \frac{d\sigma}{dE'_e d\Omega'_e d\Omega'} = \sigma_M \left(v_L \mathcal{R}^L + v_T \mathcal{R}^T + v_{TL} \mathcal{R}^{TL} + v_{TT} \mathcal{R}^{TT} \right), \quad (3)$$

where σ_M is the Mott cross section, v_K are the electron kinematical factors given in [13], and \mathcal{R}^K are the nuclear response functions, which are given as (real) linear combinations of components of the hadronic tensor

$$W^{\mu\nu} = \sum_{m_s m_B} \langle \mathbf{p}' m_s B | J^\mu(\mathbf{q}, \omega) | A \rangle^* \langle \mathbf{p}' m_s B | J^\nu(\mathbf{q}, \omega) | A \rangle, \quad (4)$$

with $J^\mu(\mathbf{q}, \omega)$ the nuclear electromagnetic current operator, and m_s, m_B are the (undetected) magnetic quantum numbers of the final unpolarized hadrons.

2.2 Nuclear and reaction models

We now give some details concerning the nuclear model of the reaction used to compute the cross section from polarized ^{39}K . For a more complete description of the model see

references [11, 14, 15]. We assume that the ground state is described as a hole (h) in the $d_{3/2}$ shell of ^{40}Ca :

$$|A\rangle = b_h^\dagger |^{40}\text{Ca}\rangle. \quad (5)$$

The ground state of the daughter nucleus ^{38}Ar is described as two holes in the $d_{3/2}$ shell of ^{40}Ca , coupled to final spin $J_B = 0$:

$$|B\rangle = [b_h^\dagger b_h^\dagger]_0 |^{40}\text{Ca}\rangle. \quad (6)$$

Thus we consider the case where the proton is ejected from the outer shell of ^{39}K . The wave function for the hole state is obtained by solving the Schrödinger equation with a Woods-Saxon potential [16].

As explained in Ref. [11], the case of a hole nucleus is not as simple as the reverse situation of a nucleus with just a single particle in the outer valence shell, for in this latter case the daughter nucleus always has $J_B = 0$ for a particle ejected from that outer shell. In the case of a hole, the residual nucleus can be in several states with different spins, and, as a result, the response \mathcal{R}^K of a one-hole nucleus is *not* the same as that for a one-particle nucleus. Yet in Ref. [11] it is shown that in the particular case where $J_B = 0$ they are proportional, with a factor $2/(2j_h + 1)$ (see eq. (82) in the above-cited reference). In the case of interest here, with $j_h = 3/2$, that factor is equal to $1/2$.

Concerning the ejected particle wave function, in the present treatment it is obtained by solving the Schrödinger equation using a complex optical potential fitted to elastic proton scattering from a variety of nuclei [17]. The partial wave (l, j) of the outgoing proton with wave number p' is normalized through the asymptotic behaviour

$$R_{lj}(r) \sim \sqrt{\frac{2M}{\pi\hbar^2 p'}} e^{-i(\sigma_l + \delta_{lj}^*)} \sin\left(p'r - \eta \log 2p'r - l\frac{\pi}{2} + \sigma_l + \delta_{lj}^*\right). \quad (7)$$

This condition reflects the boundary condition (neglecting the Coulomb potential)

$$R_{lj}(r) \sim S_{lj}^* e^{-ip'r} - e^{ip'r}, \quad (8)$$

where

$$S_{lj} = e^{2i\delta_{lj}} = \eta_{lj} e^{2i\text{Re}\delta_{lj}} \quad (9)$$

is the S -matrix partial-wave amplitude and $\eta_{lj} \leq 1$, corresponding to an absorptive potential.

Given the value $t' \equiv E' - M = \epsilon_{lj} + \omega$ of the kinetic energy of the ejected nucleon, where ϵ_{lj} is the initial-state (bound, $\epsilon_{lj} < 0$) nucleon's eigenvalue, the momentum p' is computed using relativistic kinematics

$$p' = \sqrt{E'^2 - M^2} = \sqrt{2Mt' \left(1 + \frac{t'}{2M}\right)}, \quad (10)$$

which is equivalent to making the substitution $t' \rightarrow t'(1 + \frac{t'}{2M})$ in a non-relativistic model. In addition, we use a relativized electromagnetic current which is appropriate for electron scattering calculations near the quasielastic peak [14, 18]. In this way, although based in a non-relativistic approach, our model retains many aspects of relativity which allow us to apply it for high momentum transfers.

We compute the current matrix elements by performing a multipole expansion of the current operator. Accordingly, we write the final and initial nuclear wave functions as sums of multipoles of the ejection angles and polarization angles, respectively. The sums over multipoles of the current and final states are infinite, and thus we need to truncate the expansion for values where convergence is reached. As a test of the convergence we perform the calculation of the PWIA responses in two different ways — with the multipole expansion and with the factorized expressions [7] — allowing us to fix the number of multipoles needed. From our study of response functions [11] for momenta $q \leq 700$ MeV/c, we have found that it is enough to sum up to $J = 32$ in the multipole expansion for ^{39}K .

3 Dependence of the cross section and FSI effects on the nuclear polarization

Next we present the numerical results of our calculations. In order to show the variety of FSI effects in the cross section, we have performed a calculation for different values of the angles θ^* and $\Delta\phi = \phi - \phi^*$. Here $\Omega^* = (\theta^*, \phi^*)$ are the polarization angles, or spherical coordinates of the vector $\mathbf{\Omega}^*$ in a coordinate system with \mathbf{q} in the z -axis and with the xz -plane as the electron scattering plane; ϕ is the azimuthal angle of the plane in which the ejected proton lies in this reference system.

The results are shown in figs. 1 and 2 for kinematics corresponding to the quasielastic peak and in-plane emission

$$q = 500 \text{ MeV}/c, \quad \omega = 133.5 \text{ MeV}, \quad \phi = 0, \quad \theta_e = 30^\circ, \quad (11)$$

where θ_e is the electron scattering angle. Note that for these particular kinematics, $\phi^* = -\Delta\phi$. In table 1 we give the key for obtaining the polarization angles used in each panel in figs. 1 and 2.

In fig. 1 we show 14 panels corresponding to different polarizations Ω^* . The ones at the top and bottom correspond to $\theta^* = 0$ and 180° respectively. The remaining 12 panels correspond, from top to bottom, to $\theta^* = 45, 90, 135^\circ$ and, from left to right, to $\Delta\phi = 0, 45, 90, 135^\circ$. The solid lines in this figure represent values of the cross section Σ as a function of the missing momentum p in DWIA for different polarizations contained in half of the sphere in $\mathbf{\Omega}^*$ -space; the top and bottom panels correspond to the north and south poles of the sphere. The other half of the sphere is represented in fig. 2, where again,

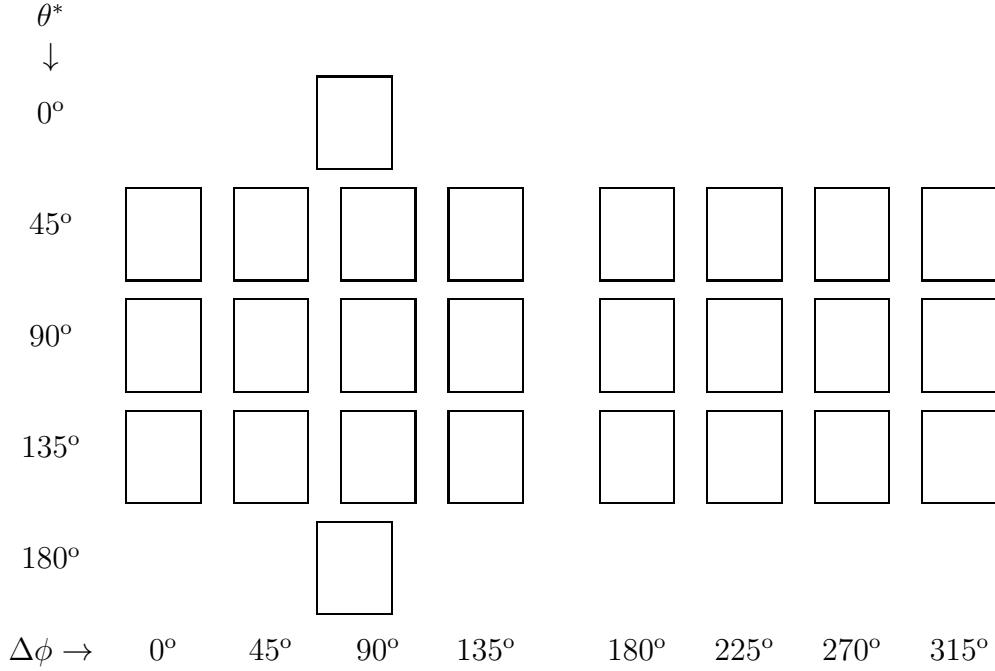


Table 1: Polarization angles for the various panels given in figs. 1 and 2

from top to bottom, $\theta^* = 45, 90, 135^\circ$, and, from left to right, $\Delta\phi = 180, 225, 270, 315^\circ$. In these figures the dashed lines are the cross sections computed in PWIA, i.e., without FSI. The dotted lines correspond to the DWIA, but including in the FSI just the central imaginary part of the optical potential, while the dash-dotted lines include in addition the central real part of the potential.

Looking at the behaviour of Σ versus the angles $(\theta^*, \Delta\phi)$ across all of the 26 panels of figs. 1–2, we see that the cross section and the relative FSI effect — i.e., the nuclear transparency, defined as the ratio between the DWIA (solid) and the PWIA (dashed) results, see eq. (33) below — both depend on the polarization angles, but in different ways. First, the PWIA results depend on the polarization angles as a consequence of the different spatial orientation of the initial nucleon momentum distribution, due to the different probability of finding a given missing momentum for different orientations. In exploring $(e, e'p)$ results of this kind, one would like to extract the spatial orientation of the momentum distribution, which could be directly measured from the dashed lines if the FSI were equal to zero.

Second, the effect of the FSI (solid lines relative to dashed lines) is quite dependent on the polarization of the nucleus. This fact suggest that the “transparency” of the nucleus to proton propagation can be maximized or minimized by selecting a particular polarization of the nucleus. One can find a great variety of FSI effects, going from small to large “transparency”. For instance, for $\theta^* = 90^\circ$, $\Delta\phi = 45^\circ$ (fig. 1), the transparency is small ~ 0.4 , while for the opposite polarization, $\theta^* = 90^\circ$, $\Delta\phi = 225^\circ$ (fig. 2), the

$$\Sigma [\text{fm}^3 \times 10^{-6}] (\theta_e = 30, \phi = 0)$$

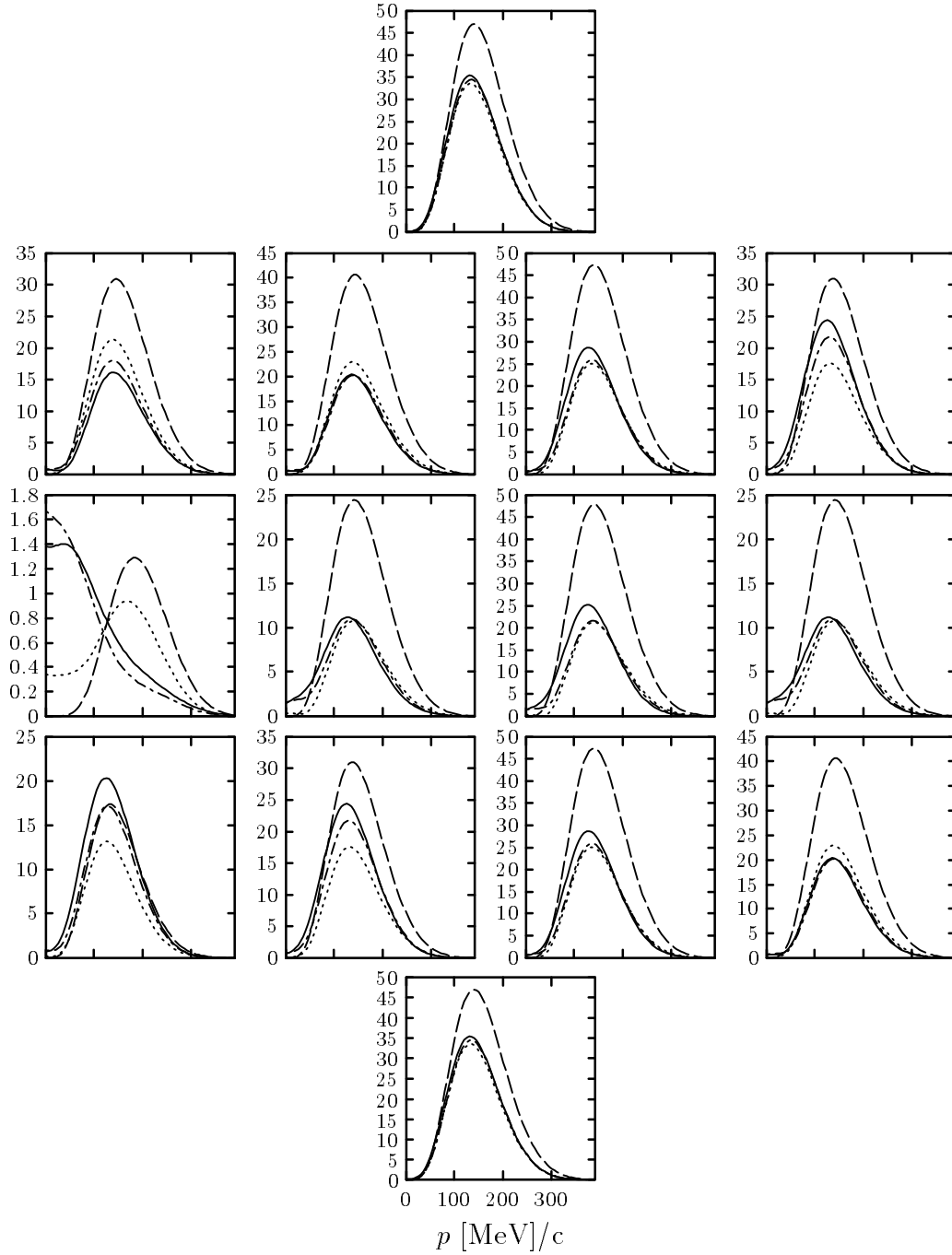


Figure 1: Cross section computed for different values of the nuclear polarization angles as shown in the first half of table 1. From top to bottom: $\theta^* = 0, 45, 90, 135, 180^\circ$. From left to right $\Delta\phi = 0, 45, 90, 135^\circ$. The meaning of the curves is the following: solid: DWIA; dashed: PWIA; dotted: DWIA but with just the imaginary part of the central optical potential; dash-dotted: DWIA without spin-orbit contributions.

$$\Sigma [\text{fm}^3 \times 10^{-6}] (\theta_e = 30, \phi = 0)$$

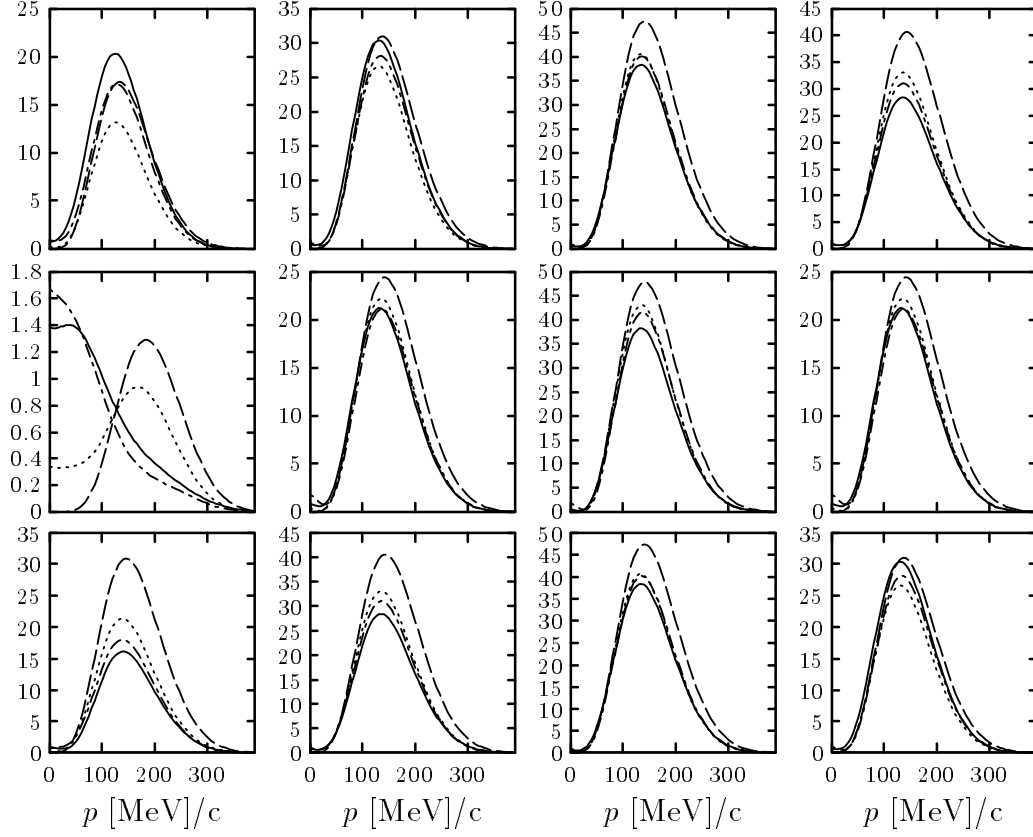


Figure 2: Cross section computed for different values of the nuclear polarization angles as shown in the second half of table 1. From top to bottom: $\theta^* = 45, 90, 135^\circ$. From left to right $\Delta\phi = 180, 225, 270, 315^\circ$. The meaning of the curves is the same as in fig. 1.

transparency is large ~ 0.9 . We also see that there are some cases, such as $\theta^* = 135^\circ$ and $\Delta\phi = 0$, for which the transparency is bigger than one.

It is apparent from these results that the nuclear transparency can change drastically in going from one polarization to the opposite, and that if one is able to understand physically the different behaviour seen for the FSI effects in figs. 1–2, then it could be possible to make specific predictions about the reaction for future experiments. The goal of the next section is to explain this dependence, at least qualitatively, by making a semi-classical, geometrical picture based on the PWIA of the new physics contained in this process, and making a quantitative analysis of the results in terms of the propagation distance of nucleons across the nucleus.

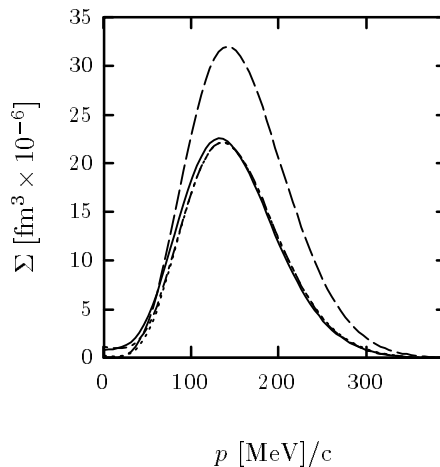


Figure 3: Unpolarized cross section. The meaning of the curves is the same as in fig. 1.

Before turning to this interpretation, let us underscore the importance of performing experiments with polarized nuclei as compared with the unpolarized case. This is clear if one examines fig. 3, where we show the unpolarized cross section given as the average of the polarized cross section $\Sigma(\Omega^*)$ over all polarization angles,

$$\Sigma_{unpol} = \frac{1}{4\pi} \int d\Omega^* \Sigma(\Omega^*). \quad (12)$$

One sees that most of the interesting behaviour displayed in figs. 1–2 goes away in the unpolarized case, and one is just able to see the averaged effect of the FSI, losing the detailed dependence of the cross section on the various polarization directions. Importantly, with polarized nuclei more restrictions can be imposed both on the nuclear modeling and on the nature of the FSI effects.

4 Polarized momentum distribution and a semi-classical picture of the reaction

In order to understand physically the results of the previous section in terms of proton propagation inside the nucleus, it is very useful to invoke the PWIA. Within this approximation one could try to make a semi-classical model of the reaction by assuming it to take place in two or more steps as follows: first a proton with (missing) momentum \mathbf{p} and energy ϵ_{ℓ_j} is knocked-out by the virtual photon and it acquires momentum \mathbf{p}' and kinetic energy $t' = \epsilon_{\ell_j} + \omega$. Second, as this high-energy nucleon traverses the nucleus it undergoes elastic and inelastic scattering. In our model, the elastic scattering is produced by the real part of the optical potential, and the inelastic scattering produces transitions of the proton into channels other than the elastic one, which can be phenomenologically treated as absorption due to the imaginary part of the optical potential.

The important point here is that the nucleus is polarized in a specific direction. Accordingly, the initial-state nucleon can be localized in an oriented (quantum) orbit. From the knowledge of this orbit and of the missing momentum one can predict the most probable location of the struck proton, i.e., computing the expectation value of its position before the reaction takes place, and therefore one can specify the quantity of nuclear matter that the proton must cross before exiting from the nucleus with momentum \mathbf{p}' .

4.1 Distribution of a $d_{3/2}$ wave

We illustrate the case of a particle in a $d_{3/2}$ wave, because in the extreme shell model employed here it is the relevant state for the reaction $^{39}\vec{\text{K}}(e, e'p)^{38}\text{Ar}_{g.s.}$, in which the residual ^{38}Ar nucleus in its ground state is described as two protons in the $d_{3/2}$ orbit coupled to total angular momentum $J_B = 0$. For this model of the reaction it is the third proton in the $d_{3/2}$ orbit which carries the angular momentum of the initial nucleus ^{39}K . The wave function for a single particle in the $d_{3/2}$ shell polarized in the z -direction ($\mathbf{\Omega}^* = \mathbf{e}_3$; i.e., the particle is in the $|\frac{3}{2}\frac{3}{2}\rangle$ state), is given by

$$\begin{aligned} |\frac{3}{2}\frac{3}{2}\rangle &= \langle 21\frac{1}{2}\frac{1}{2} | \frac{3}{2}\frac{3}{2} \rangle Y_{21}(\theta, \phi) R(r) | \uparrow \rangle + \langle 22\frac{1}{2} - \frac{1}{2} | \frac{3}{2}\frac{3}{2} \rangle Y_{22}(\theta, \phi) R(r) | \downarrow \rangle \\ &= \psi_1 | \uparrow \rangle + \psi_2 | \downarrow \rangle. \end{aligned} \quad (13)$$

Inserting the appropriate values for the Clebsch-Gordan coefficients and the spherical harmonics we obtain for the spinor wave functions

$$\psi_1 = -\sqrt{\frac{3}{8\pi}} \sin \theta \cos \theta e^{i\phi} R(r) \quad (14)$$

$$\psi_2 = -\sqrt{\frac{3}{8\pi}} \sin^2 \theta e^{2i\phi} R(r). \quad (15)$$

Here the angles (θ, ϕ) are the spherical coordinates of the particle's position \mathbf{r} and $R(r)$ is its radial wave function. The total wave function in momentum space (Fourier transform) has the same angular dependence with respect to the angles of the missing momentum \mathbf{p} , the only differences being that the radial wave function is in momentum space and a global phase enters. The spatial distribution is then given by the single-particle probability density

$$\rho(\mathbf{r}) = |\psi_1|^2 + |\psi_2|^2 = \frac{3}{8\pi} \sin^2 \theta |R(r)|^2. \quad (16)$$

Taking into account the form of the radial wave function for the $d_{3/2}$ wave, we can see that the particle is distributed around the center of the nucleus in a toroidal-like orbit as shown schematically in fig. 4 (upper part). In a semi-classical picture of the bound state, we can imagine the particle performing a rotatory orbit within the torus in a counter-clock sense. The sense of rotation can be deduced from the direction of the angular momentum, namely it has to point predominantly along the z -direction since the nucleon has spin-1/2, and the value $J_z = \frac{3}{2}$ can only be reached if the orbital angular momentum also points in the positive z -direction. This idea is corroborated by the model introduced in next section for the local momentum of the nucleon. The momentum distribution, which can be obtained using the Fourier transform of the above wave function, has a similar shape in momentum space. The shape of the distribution for arbitrary polarization Ω^* is just a rotation of the above distribution, as also shown in fig. 4 (bottom).

4.2 Expectation value of the position for a given missing momentum

Having established the three-dimensional shape of the nucleon orbit, the next step is to localize the particle within the orbit for a given value of the missing momentum \mathbf{p} . To this end, from elementary quantum mechanics we first recall that the probability current for a given wave function, $\psi(\mathbf{r})$, can be written as

$$\mathbf{j}(\mathbf{r}) = \frac{1}{M} \text{Re} \psi^\dagger(\mathbf{r})(-i\nabla)\psi(\mathbf{r}). \quad (17)$$

In a semi-classical picture from this one can define the local velocity $\mathbf{v}(\mathbf{r})$ of the particle as

$$\mathbf{j}(\mathbf{r}) = \mathbf{v}(\mathbf{r})\rho(\mathbf{r}) \quad (18)$$

with the particle density

$$\rho(\mathbf{r}) = \psi^\dagger(\mathbf{r})\psi(\mathbf{r}). \quad (19)$$

As a consequence, a local momentum for the particle can be defined as the expected value of the momentum operator $\hat{\mathbf{p}} = -i\nabla$ in the following way:

$$\mathbf{p}(\mathbf{r}) = M\mathbf{v}(\mathbf{r}) = \frac{\text{Re} \psi^\dagger(\mathbf{r})(-i\nabla)\psi(\mathbf{r})}{\psi^\dagger(\mathbf{r})\psi(\mathbf{r})}. \quad (20)$$

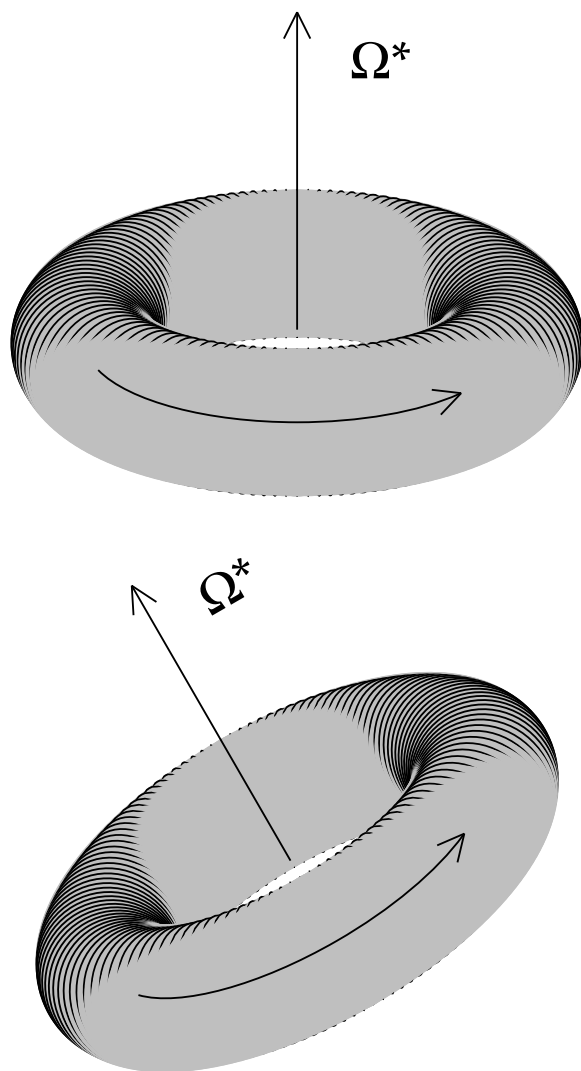


Figure 4: Pictorial representation of the spatial distribution of a proton in the $d_{3/2}$ shell, shown as a torus-like distribution for two different polarizations.

This equation gives us the expected value of momentum for a given position. In order to obtain the expectation value of the *position* for a given value of the *missing momentum* \mathbf{p} , we repeat the above procedure, now working in momentum space. Accordingly, we employ the Fourier transform $\tilde{\psi}(\mathbf{p})$ of the wave function and the position operator in momentum space $\hat{\mathbf{r}} = i\nabla_p$ to define the local position of the nucleon in the orbit for momentum \mathbf{p} in the following way:

$$\mathbf{r}(\mathbf{p}) = \frac{\text{Re } \tilde{\psi}^\dagger(\mathbf{p})(i\nabla_p)\tilde{\psi}(\mathbf{p})}{\tilde{\psi}^\dagger(\mathbf{p})\tilde{\psi}(\mathbf{p})}. \quad (21)$$

This is a well-defined vector which represents the most probable location of a particle with momentum \mathbf{p} when it is described by a wave function ψ . Henceforth $\mathbf{r}(\mathbf{p})$ represents the position of the particle in the orbit in the present semi-classical model.

For the case of interest here of the $d_{3/2}$ orbit polarized in the z -direction, we compute the position $\mathbf{r}(\mathbf{p})$ by using the wave function given in eqs. (13–15) in momentum space:

$$\tilde{\psi}^\dagger(\mathbf{p})i\nabla_p\tilde{\psi}(\mathbf{p}) = \tilde{\psi}_1^*i\nabla_p\tilde{\psi}_1 + \tilde{\psi}_2^*i\nabla_p\tilde{\psi}_2, \quad (22)$$

where now $\tilde{\psi}_1, \tilde{\psi}_2$ are the Fourier transforms of the up and down spinor wave functions. Using spherical coordinates, one can compute the gradient and take the real part

$$\text{Re } \tilde{\psi}^\dagger(\mathbf{p})i\nabla_p\tilde{\psi}(\mathbf{p}) = -\frac{3}{8\pi} \frac{|\tilde{R}(p)|^2}{p} \sin\theta(1 + \sin^2\theta)\hat{\phi}, \quad (23)$$

where (θ, ϕ) are the spherical coordinates of the missing momentum \mathbf{p} , $\tilde{R}(p)$ is the radial wave function in momentum space, and $\hat{\phi}$ is the unit vector in the azimuthal direction. As we see, upon dividing by the momentum distribution (given by eq. (16), but in momentum space)

$$\tilde{\psi}^\dagger(\mathbf{p})\tilde{\psi}(\mathbf{p}) = \frac{3}{8\pi} \sin^2\theta|\tilde{R}(p)|^2, \quad (24)$$

the radial dependence in the numerator and denominator goes away, and we obtain an expectation value of position which is independent of the radial wave function — namely, just a geometrical quantity which is characteristic of the $d_{3/2}$ wave:

$$\mathbf{r}(\mathbf{p}) = -\frac{1 + \sin^2\theta}{p \sin\theta} \hat{\phi}. \quad (25)$$

This expression has been obtained for the polarization direction $\boldsymbol{\Omega}^* = \mathbf{e}_3$, namely, in the z -direction. For a general polarization vector $\boldsymbol{\Omega}^*$ we just perform a rotation of the vector $\mathbf{r}(\mathbf{p})$. Introducing the angle θ_p^* between \mathbf{p} and $\boldsymbol{\Omega}^*$,

$$\mathbf{p} \cdot \boldsymbol{\Omega}^* = p \cos\theta_p^*, \quad (26)$$

we can write the nucleon position in a way which is valid for any polarization:

$$\mathbf{r}(\mathbf{p}) = -\frac{1 + \sin^2\theta_p^*}{p^2 \sin^2\theta_p^*} \boldsymbol{\Omega}^* \times \mathbf{p}. \quad (27)$$

Also, in order to illustrate the concept of momentum flow for the nucleon orbit introduced above, we write down the corresponding expression for the expectation value of momentum at a specific position \mathbf{r} :

$$\mathbf{p}(\mathbf{r}) = \frac{1 + \sin^2 \theta_r^*}{r^2 \sin^2 \theta_r^*} \boldsymbol{\Omega}^* \times \mathbf{r}, \quad (28)$$

where now θ_r^* is the angle between \mathbf{r} and $\boldsymbol{\Omega}^*$. Note that here there is an extra minus sign with respect to eq. (27) coming from the different correspondences $\mathbf{r} \rightarrow i\nabla_p$ and $\mathbf{p} \rightarrow -i\nabla_r$. Eq. (28) corresponds classically to a circular movement (orbit) around the rotation axis given by the polarization $\boldsymbol{\Omega}^*$.

4.3 Applications to the $(e, e'p)$ reaction

As a first example of the utility of the above definitions for a physical interpretation of the results given in figs. 1–2, let us consider the case of the $(e, e'p)$ reaction with the ^{39}K nucleus polarized in the $-y$ direction ($\boldsymbol{\Omega}^* = -\mathbf{e}_2$), given by the angles $\theta^* = 90^\circ$, $\phi^* = -90^\circ \implies \Delta\phi = 90^\circ$. The kinematics are illustrated in fig. 5(a). Therein, the momentum transfer points in the z -direction and we show the missing-momentum vector \mathbf{p} corresponding to the maximum of the momentum distribution, $p \sim 140$ MeV/c. For $\omega \sim 133.5$ MeV (near the quasielastic peak) the momentum of the ejected proton \mathbf{p}' is also shown in the picture. For $\boldsymbol{\Omega}^*$ pointing in the $-y$ direction, the semi-classical orbit lies in the xz -plane and follows a counter-clockwise direction of rotation. For these conditions, the most probable position of the proton before the interaction is indicated with a black dot near the bottom of the orbit. As the particle is going up with momentum \mathbf{p}' after the interaction with the virtual photon, it has to cross all of the nucleus (not shown in the figure) and exit it by the opposite side; thus one expects that the FSI will be large in this situation, as shown in the corresponding panel of fig. 1.

In fig. 5(b) we show the picture for the opposite polarization in the y -direction ($\boldsymbol{\Omega}^* = \mathbf{e}_2$), with angles $\theta^* = 90^\circ$, $\phi^* = 90^\circ \implies \Delta\phi = 270^\circ$. In this case the nucleon distribution in the orbit is the same as in (a), but the rotation direction is the opposite, the sense being now clockwise. Hence now it is more probable for the nucleon to be located near the upper part of the orbit. As the nucleon is still going up with the same momentum \mathbf{p}' , the distance that it has to travel through the nucleus is much smaller than in case (a), and hence one expects small FSI effects, namely, what is seen in the results of fig. 2.

As we can see, we have arrived at a very intuitive physical picture of why the FSI effects differ for different orientations of the nuclear spin: the polarization direction fixes the orientation of the nucleon distribution (or in semi-classical language, the nucleon orbit). For a given value of the missing momentum one can locate the particle in a definite position within the orbit, and therefore within the nucleus. As the particle leaves the nucleus with known momentum \mathbf{p}' , one can immediately determine the quantity of nuclear matter that it has to cross before exiting. Now we generalize the above examples to all of the polarizations considered in this work.

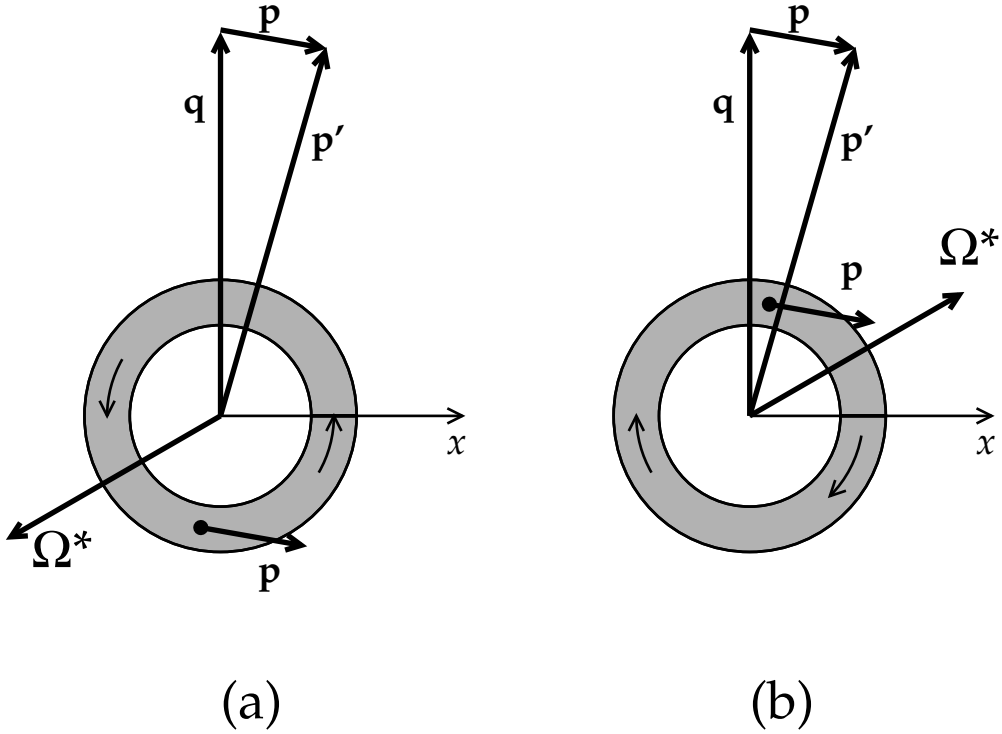


Figure 5: Semi-classical orbit and location of the proton for the given kinematics and for the nuclear polarization (a) in the $-y$ direction, and (b) in the y -direction. In the two cases the final nucleon leaves the nucleus with momentum \mathbf{p}' . In case (a) the nucleon is in the lower part of the orbit and has to cross a large quantity of nuclear matter, resulting in large FSI, whereas in case (b) the proton is in the upper part of the orbit and crosses a small amount of matter, resulting in small FSI.

In fig. 6 we show a general geometrical picture of the position of the proton before exiting the nucleus, computed using eq. (27) for the same kinematical conditions of figs. 1 and 2 and for all of the 26 polarizations considered in this work. The value of the missing momentum in fig. 6 corresponds to the maximum of the cross section (approximately located at the maximum of the momentum distribution $p \sim 140$ MeV/c).

In order to make the visualization of fig. 6 clearer, we have chosen to have the z -axis in the direction of the final momentum \mathbf{p}' ; that is, in all cases the final proton is going up. Each circle represents the nuclear interior with radius $R \sim 3.8$ fm and the position of the proton before the impact is shown with a black circle. Each gray circle in fig. 6 corresponds to a different nuclear polarization, which means a different orientation of the $d_{3/2}$ orbit and a different position \mathbf{r} for the nucleon. The x -axis in each one of the circles has been chosen to be in the plane generated by the vectors \mathbf{p}' and \mathbf{r} in order to present the picture as a bi-dimensional plot. The arrows represent the vector \mathbf{p}' .

Each gray circle in fig. 6 corresponds to one of the 26 panels in figs. 1–2 and they are

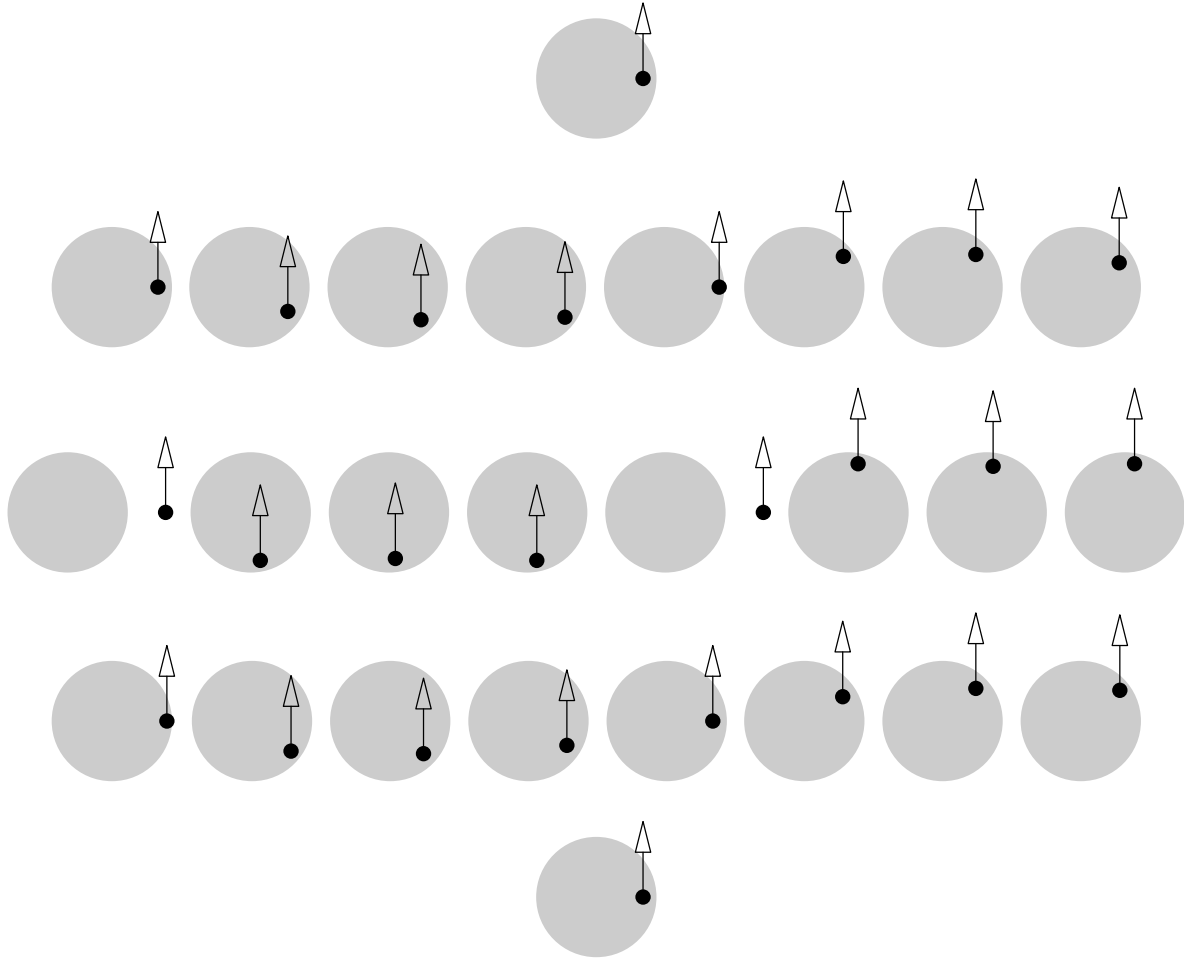


Figure 6: Initial position of the proton within the nucleus for each of the polarizations of figs. 1–2 and table 1, computed using eq. (27). In each case the reference system has been chosen so that the final momentum is going up and the position is in the plane of the figure. In the cases where the proton is in the lower half of the nucleus the FSI effects are found to be large in fig. 1, while the situations where the proton is in the upper half, the FSI effects are small. The re-scattering effects produced by the real and spin-orbit potentials are important only when the proton is near the “equator” of the nucleus and close to its surface, initially with large impact parameter.

arranged in the same way as indicated in table 1: the upper and lower circles correspond to the polarizations $\theta^* = 0$ and $\theta^* = 180^\circ$ respectively. Each one of the remaining three rows correspond, from up to down, to $\theta^* = 45, 90, 135^\circ$, respectively, while each one of the eight columns corresponds to a value of $\Delta\phi = 0, 45, 90, 135, 180, 225, 270, 315^\circ$. The computed values of $|\mathbf{r}(\mathbf{p})|$ are given in table 2.

As a first qualitative analysis of the systematics of the FSI, we can see by comparing the dashed (PWIA) and solid lines (DWIA) of figs. 1–2, and looking at fig. 6, that in the cases where the FSI effects are large —predominantly in fig. 1— the nucleon is likely to be located somewhere in the lower half of the nucleus, going up in all cases, and traversing a large amount of nuclear matter. This happens for $\Delta\phi = 45, 90, 135^\circ$ and the most extreme cases correspond to $\theta^* = 90^\circ$, for which the proton is at the bottom of the nucleus in fig. 6 and has to travel the largest distance before exiting the nucleus through the upper surface.

On the other hand, for $\Delta\phi = 225, 270, 315^\circ$ (fig. 2), the nucleon is located in the upper half of the nucleus, and it is still going up. Accordingly, the quantity of nuclear matter that is crossed is small and the FSI effects are also small, as seen in fig. 2. The most extreme cases happen again for $\theta^* = 90^\circ$, where the nucleon is initially near the top of the nucleus and for which a rather small portion of the nucleus is traversed, the FSI effects being the smallest in fig. 2 for these cases.

Finally, we find intermediate cases where the nucleon is somewhere near the “equator” of the nucleus, namely $\theta^* = 0, 180^\circ$ (i.e., L and $-L$ polarizations), where the FSI effects are in between the extreme cases discussed above, and also for $\Delta\phi = 0, 180^\circ$, where the above semi-classical picture of the process is difficult to apply.

Consider the most extreme “outsider” case, $\theta^* = 90^\circ$, $\Delta\phi = 0$, for which $r(\mathbf{p}) = 5.6$ fm and so the nucleon is “outside” of the nuclear surface (fig. 6). Actually what happens in this case is that the missing-momentum vector is almost perpendicular to the plane of the momentum distribution, as seen in fig. 7. In other words, the probability of finding a proton with momentum \mathbf{p} is very small; so the cross section is also very small (less than 10% of the cross sections for the other polarizations shown in fig. 1) and therefore the FSI effects are maximized for these conditions. The reason for the computed proton position being outside of the nucleus for this polarization is that the angle θ_p^* between \mathbf{p} and $\mathbf{\Omega}^*$ is very small and hence the denominator in eq. (27) is small, resulting in a large value of $\mathbf{r}(\mathbf{p})$.

Two other interesting “outsider” cases correspond to the polarizations $\Delta\phi = 0$ and $\theta^* = 45, 135^\circ$, respectively. In both cases the nucleon near the “equator” of the nucleus and close to its surface (see fig. 6). In the first case the FSI effects are large and produce a reduction of the PWIA cross section by a factor $\sim 1/2$ (fig. 1). In the second case the FSI produce a small *increase* of the cross section (see also fig. 1). The only difference between these two polarizations in our geometrical picture (fig. 6) is the distance of the proton to the center of the nucleus: $r = 2.77$ fm and $r = 3.28$ fm respectively. As in both cases the proton is practically at the nuclear surface, effects other than absorption are

θ^* [°]	$\Delta\phi$ [°]	$r(\mathbf{p})$ [fm]	s [fm]	T	$\log T$	λ [fm]
0.	0.	2.799	2.570	.707	-.347	7.411
45.	0.	2.768	2.604	.686	-.376	6.920
45.	45.	2.712	4.492	.561	-.579	7.759
45.	90.	2.799	5.208	.527	-.640	8.136
45.	135.	2.970	4.820	.568	-.566	8.519
45.	180.	3.282	1.916	.748	-.290	6.608
45.	225.	2.970	1.166	.856	-.156	7.488
45.	270.	2.799	1.268	.848	-.165	7.703
45.	315.	2.712	1.577	.802	-.221	7.144
90.	0.	5.860	.000	.700	-.356	.000
90.	45.	2.959	6.655	.442	-.816	8.155
90.	90.	2.799	6.552	.445	-.810	8.087
90.	135.	2.959	6.655	.442	-.816	8.155
90.	180.	5.860	.000	.700	-.356	.000
90.	225.	2.959	.854	.904	-.101	8.429
90.	270.	2.799	1.008	.893	-.113	8.899
90.	315.	2.959	.854	.904	-.101	8.429
135.	0.	3.282	1.916	.748	-.290	6.608
135.	45.	2.970	4.820	.568	-.566	8.519
135.	90.	2.799	5.208	.527	-.640	8.136
135.	135.	2.712	4.492	.561	-.579	7.759
135.	180.	2.768	2.604	.686	-.376	6.920
135.	225.	2.712	1.577	.802	-.221	7.144
135.	270.	2.799	1.268	.848	-.165	7.703
135.	315.	2.970	1.166	.856	-.156	7.488
180.	0.	2.799	2.570	.707	-.347	7.411

Table 2: We show several quantities computed within our model for all of the nuclear polarization angles considered, and for the missing momentum at the maximum of the cross section in each case. From third to seventh columns we show: the computed position of the proton $r(\mathbf{p})$ within the orbit; the length of the nucleon path s within the nucleus for nuclear radius $R = 3.8$ fm; the nuclear transparency T and its logarithm computed with just the imaginary part of the central optical potential in the FSI; the mean free path computed as $\lambda = -s/\log T$.

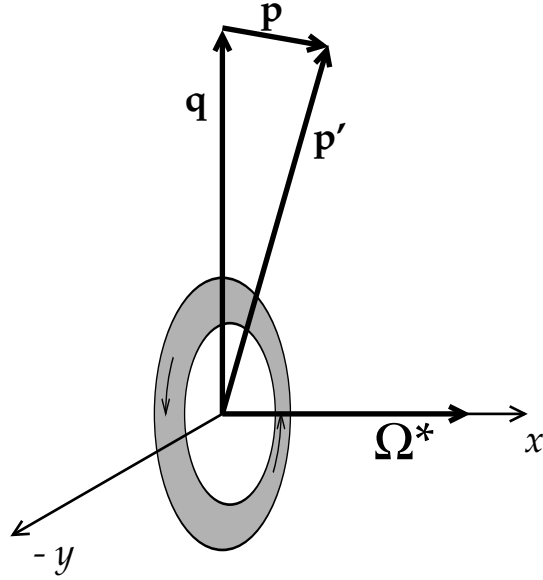


Figure 7: Nucleon orbit for x -polarization. For the present kinematics the missing momentum is almost perpendicular to the orbit plane, the corresponding probability of finding such a proton within the orbit is very small, and the FSI effects are relatively large.

at the same level of importance, namely, scattering by the real part of the potential and effects relating to the spin-orbit interaction.

In fact, the DWIA results in figs. 1–2 have been computed using an optical potential of the type

$$V = V_c + V_{ls} \vec{l} \cdot \vec{s} \quad (29)$$

with V_c the central and V_{ls} the spin-orbit part of the potential, both being complex functions of r :

$$V_c = U_c + iW_c \quad (30)$$

$$V_{ls} = U_{ls} + iW_{ls}. \quad (31)$$

In figs. 1–2 we also show with dotted lines the cross section computed using only a purely absorptive central potential in the final state, i.e., taking $V = iW_c$ or making $U_c = V_{ls} = 0$. In contrast, the dash-dotted lines in the figures correspond to a calculation without the spin-orbit potential, i.e., $V_{ls} = 0$.

In going from the dotted to the dash-dotted and to the solid lines in figs. 1–2, we see that in general the major part of the reduction of the cross section by the FSI is produced by the central absorptive part of the potential iW_c (dotted lines). The inclusion of the real part U_c (dash-dotted lines) produces a small effect in the cross section for most of the cases and the same happens for the inclusion of the spin-orbit V_{ls} (solid).

The cases having larger effects in the cross section due to the real and spin-orbit interactions always correspond in fig. 6 to geometries in which the initial nucleon is located near the “equator” and to the right of the nucleus, i.e., initially with large impact parameter, close to the nuclear surface and with final momentum \mathbf{p}' tangent to the surface. In such situations, scattering processes and spin-orbit interactions in the surface are maximized, the non-absorptive part of the interaction produces deviations of the initial trajectory into or out of the nucleus, and as a consequence more or less additional absorption is produced.

Two examples are used to illustrate this point. First, the $\Delta\phi = 0, \theta^* = 45^\circ$ case shows a situation where the real and spin-orbit potentials produce absorption additional to that provided by the imaginary part (fig. 1). Second, the $\Delta\phi = 0, \theta^* = 135^\circ$ case is one where the nucleon is closer to the nuclear surface and scattering processes appear to push it farther (fig. 1) out, so that the amount of absorption produced by the total central potential $V_c = U_c + iV_c$ is negligible (dash-dotted lines in the corresponding panel). In addition, the spin-orbit interaction produces an enhancement of the PWIA results for this polarization (solid lines), making the total transparency bigger than one.

Clearly the surface interactions and scattering processes just discussed vitiate the possibility of a complete analysis of the FSI for all of the polarizations using a single attenuation parameter such as a nuclear “mean free path” (MFP). However, the understanding gained above does indicate how one could extract such a parameter from a selection of the present results. We again start with the semi-classical concept of a nucleon orbit. In fact, from fig. 6 it is possible to compute the distance s that the nucleon travels across the nucleus before exiting by choosing some appropriate value for the nuclear radius R . A model of exponential attenuation of the cross section due to nuclear absorption (or quantum transitions to channels other than the elastic one) can be crafted in the following way:

$$\Sigma_{DWIA} \simeq \Sigma_{PWIA} e^{-s/\lambda}, \quad (32)$$

where λ is the MFP and s is the distance of the nucleon trajectory within the nucleus. Within this crude approximation, the nuclear transparency, defined as the ratio between the DWIA and PWIA results, can be written as

$$T \equiv \frac{\Sigma_{DWIA}}{\Sigma_{PWIA}} \simeq e^{-s/\lambda}. \quad (33)$$

In fig. 8 we show the nuclear transparency as a function of the distance s to the nuclear surface, computed for each one of the polarizations of figs. 1–2. We have computed the transparency at the maximum of the cross section, where for the FSI we have used just the imaginary part of the optical potential $V = iW_c$, without the spin-orbit term (i.e., we have used as Σ_{DWIA} the dotted lines in figs. 1–2). The numerical values of s and the transparency are given in table 2.

In fig. 8 we see that the dependence of $\log T$ can in fact be approximated by a straight line with slope $-1/\lambda$, thus allowing one to extract an effective MFP in finite nuclei.

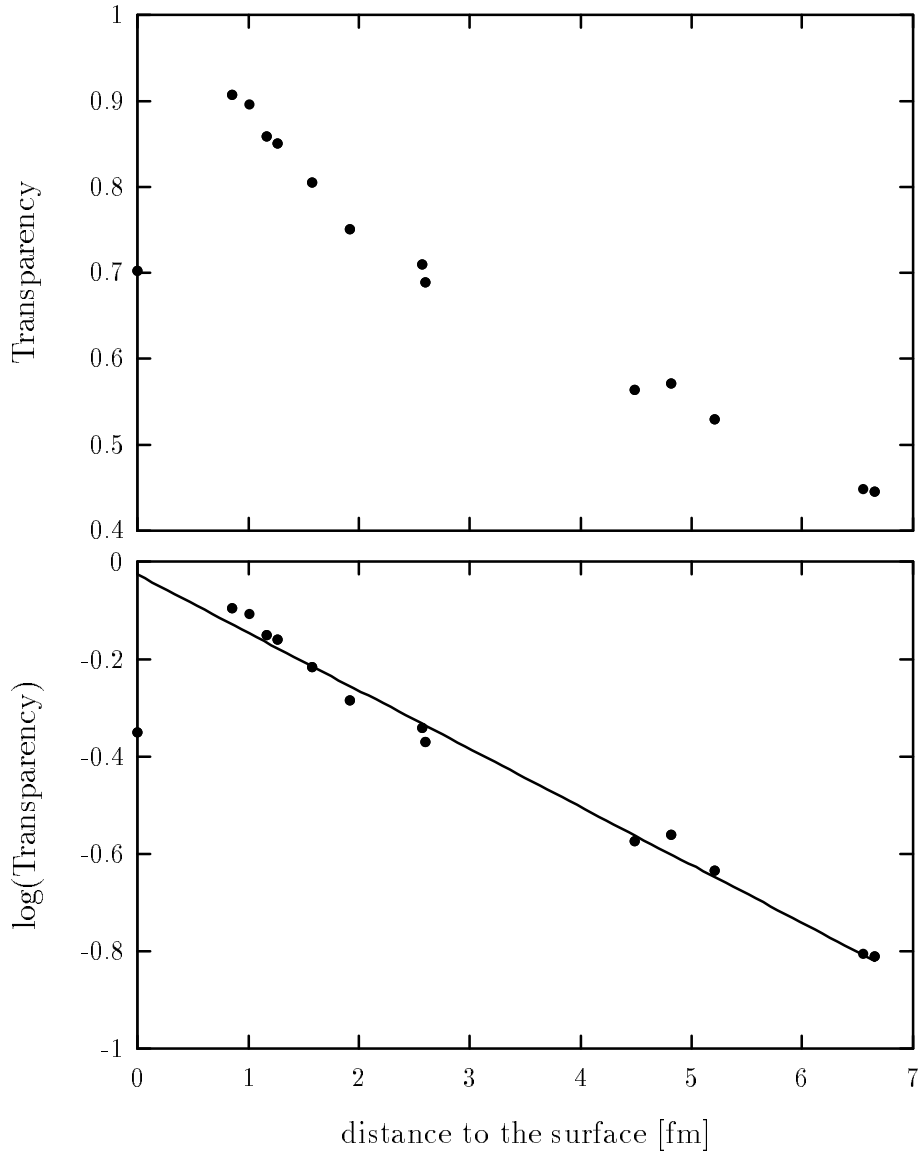


Figure 8: Nuclear transparency as a function of the nucleon path s within the nucleus for the different polarizations considered in this work. The FSI only include the imaginary part of the central optical potential. The $\log T$ dependence can be parametrized with a straight line with slope $-1/\lambda$, where λ is the mean free path. The point with $s = 0$ is the “outsider” case of fig. 7, which cannot easily be explained within the semi-classical model.

In the last column of table 2 we also show the value of the MFP extracted from each polarization as $\lambda = -s/\log T$. This value is within the range 6.6 to 8.9 fm, with the exception of the two “outsider” cases where the proton is beyond the surface. This gives an averaged value of $\langle\lambda\rangle = 7.7$ fm. By performing a linear regression we obtain a MFP of $\lambda_{lr} = 8.4$ fm.

The values for the MFP given in table 2 depend on the value chosen for the nuclear radius R . The value $R = 3.8$ fm chosen above corresponds to the point $r_{1/4}$ for which the nuclear density $\rho(r)$ is 25% of $\rho(0)$. In table 3 we present a study of the dependence of λ as a function of the nuclear radius. The length of the nucleon path through the nucleus increases with the nuclear radius, so the averaged MFP increases with R . For small radius $R = r_{1/2} = 3.2$ fm, the value of $\langle\lambda\rangle = 4.9$ fm, close to the value that is used for nuclear matter. For this value of the radius the proton is not yet completely outside of the nucleus, although it is in the surface region; however, for finite nuclei a somewhat larger value of R would be more reasonable, since the full density of nuclear matter is not attained with finite nuclei. In the results of table 2 we have defined the nuclear surface as the region between $r_{1/2}$ and $r_{1/4}$.

On the other hand, the values λ_{lr} obtained with a linear regression are quite independent of the radius in the region between $r_{1/2}$ and $r_{1/10}$. Consequently we believe that the value of $\lambda \sim 8.5$ fm obtained in this way is appropriate as a “model independent” definition of the MFP for protons in finite nuclei under the conditions of the present work.

R	$\langle\lambda\rangle$	λ_{lr}	$\rho(R)/\rho(0)$
3.1	4.3	8.6	
3.2	4.9	8.5	0.50
3.5	6.2	8.6	
3.6	6.7	8.5	0.30
3.8	7.7	8.4	0.25
3.9	8.2	8.4	0.20
4.3	10.1	8.3	0.10

Table 3: Dependence of the computed mean free path on the nuclear radius R . The second column is the MFP computed for each point in fig. 8 and then averaged. The third column is the MFP obtained with a linear regression of fig. 8 and the fourth column gives the density ratio for some of the R -values. In table 2 and fig. 8 we have used the value $R = 3.8$ fm corresponding to a nuclear density which is 25% of the value at the origin.

Finally, note that the above results for the MFP and nuclear transparency have been obtained using just the imaginary part of the central optical potential, whereas in an experiment one cannot separate the different pieces of the FSI. The results of shown in figs. 1–2 indicate that there are situations where the real and spin-orbit pieces of the FSI are of little importance in the cross section, these situations corresponding to nuclear

polarizations for which the impact parameter of the initial nucleon is small. Therefore, if one considers just these cases, it is still possible to extract the MFP with small error.

5 Conclusions

In this paper we have studied the reaction $^{39}\text{K}(e, e'p)^{38}\text{Ar}_{\text{gs}}$ for polarized ^{39}K . The corresponding cross section has been computed within the framework of the shell model and the FSI have been taken into account by using an optical potential in the final state. The goal of the present paper has been to study the dependence of the FSI as a function of the nuclear polarization direction and to introduce a physical picture of the results in order to understand the different effects seen in the cross section.

The argument to explain the FSI effects is based on the PWIA and it has been illustrated by introducing the semi-classical concept of a nucleon orbit within the nucleus. In fact, for given kinematics (momentum transfer, missing momentum and polarization angles) we can fix the nucleon orbit *including its expected direction of motion and the expectation value of the position of the nucleon within the nucleus before the interaction*. From this information we have computed the length of the path that the nucleon travels across the nucleus for each polarization.

Our results show that when the FSI effects are large the computed nucleon path through the nucleus is also large, whereas the opposite happens when the FSI effects are small. The importance of the real and spin-orbit pieces of the optical potential increases with the impact parameter of the initial nucleon with respect to the emission direction. Thus, by selecting the appropriate nuclear polarization, one can reduce or enhance the FSI effects and the importance of the real and spin-orbit pieces. Such control should prove to be very useful in analyzing the results from future experiments with polarized nuclei.

Finally, within our model we have studied the nuclear transparency as a function of the length of the nucleon path, providing a way of obtaining a mean free path for protons in finite nuclei.

In summary we have understood in some depth the role of FSI in $(e, e'p)$ reactions from polarized nuclei. Since by flipping the nuclear polarization one can go from big to small FSI effects, this opens the possibility of using this kind of reaction to vary the roles played by the FSI, and thus to distinguish their effects from other issues of interest, such as the nature of nuclear structure and the electromagnetic nuclear current.

Finally, we note that in this work we have analyzed the total cross section for unpolarized electrons. It is desirable to extend this study to polarized electrons where other spin observables and asymmetries enter. Work along these lines is in progress.

Acknowledgments

The authors thank J.A. Caballero, S. Jeschonnek, R. Cenni and A. Molinari for helpful discussions on the FSI.

This work is supported in part by funds provided by the U.S. Department of Energy (D.O.E.) under cooperative agreement #DE-FC01-94ER40818, in part by DGICYT (Spain) under Contract No. PB92-0927 and the Junta de Andalucía (Spain) and in part by NATO Collaborative Research Grant #940183.

References

- [1] D. F. Geesaman *et al.*, Phys. Rev. Lett. **63** (1989) 734.
- [2] G. Garino *et al.*, Phys. Rev. **C45** (1992) 780.
- [3] S. Frullani and J. Mougey in *Advances in Nuclear Physics*, (J. W. Negele and E. W. Vogt, Eds.), Vol. 14, Plenum Press, New York, 1984.
- [4] N.C.R. Making *et al.*, Phys. Rev. Lett. **72** (1994) 1986.
- [5] T.G. O'Neill *et al.*, Phys. Lett. **B351** (1995) 87.
- [6] B. Blättel, G. Baym, L.L. Frankfurt and M. Strikman, Phys. Rev. Lett. **70** (1993) 896.
- [7] J.A. Caballero, T.W. Donnelly and G.I. Poulis, Nucl. Phys. **A555** (1993) 709.
- [8] J.A. Caballero, T.W. Donnelly, G.I. Poulis, E. Garrido and E. Moya de Guerra, Nucl. Phys. **A577** (1994) 528.
- [9] E. Garrido, J.A. Caballero, E. Moya de Guerra, P. Sarriguren and J.M. Udías, Nucl. Phys. **A584** (1995) 256.
- [10] J.A. Caballero, E. Garrido, E. Moya de Guerra, P. Sarriguren, J.M. Udías, Ann. Phys. **239** (1995) 351.
- [11] J.E. Amaro and T.W. Donnelly Ann. Phys. (N.Y.) **263** (1998) 56.
- [12] S. Boffi, C. Giusti and F.D. Pacati, Nucl. Phys **A476** (1988) 617.
- [13] A.S. Raskin and T.W. Donnelly, Ann. Phys. (NY) **191** (1989) 78.
- [14] J.E. Amaro, J.A. Caballero, T.W. Donnelly, A.M. Lallena, E. Moya de Guerra and J.M. Udías, Nucl. Phys. **A602** (1996) 263.

- [15] J.E. Amaro, J.A. Caballero, T.W. Donnelly and E. Moya de Guerra, Nucl. Phys. **A611** (1996) 163.
- [16] J.E. Amaro, C. García-Recio and A.M. Lallena Nucl. Phys. **A567** (1994) 701; S. Moraghe, J.E. Amaro, C. García-Recio and A.M. Lallena, Nucl. Phys. **A576** (1994) 553.
- [17] P. Schwandt *et al.*, Phys. Rev. **C26** (1982) 55.
- [18] J.E. Amaro, M.B. Barbaro, J.A. Caballero, T.W. Donnelly and A. Molinari, to be published in Nucl. Phys. A.